Mon. Not. R. Astron. Soc. **000**, 000–000 (0000) Printed 26 May 2014 (MN LATEX style file v2.2)

Cosmological constraints from the CFHTLenS shear measurements using a new, accurate and flexible way of predicting nonlinear mass clustering.

Raul E. Angulo[1] & Stefan Hilbert[2,3].
[1] *Centro de Estudios de Física del Cosmos de Aragón, Plaza San Juan 1, Planta-2, 44001, Teruel, Spain.*
[2] *Exzellenzcluster Universe, Boltzmannstr. 2, 85748 Garching, Germany*
[3] *Max-Planck-Institut für Astrophysik, Karl-Schwarzschild-Str. 1, 85748 Garching, Germany.*

26 May 2014

ABSTRACT
We explore the cosmological constraints from cosmic shear using a new way of modelling the non-linear matter correlation functions. The new formalism extends the method of Angulo & White (2010), which manipulates outputs of N-body simulations to represent the three-dimensional nonlinear mass distribution in different cosmological scenarios. We show that predictions from our approach for shear two-point correlations at 1 to 300 arcmin separations are accurate at the $\sim 10\%$ level, even for extreme changes in cosmology. For moderate changes, with target cosmologies similar to that preferred by analyses of recent Planck data, the accuracy is close to $\sim 5\%$. We combine this approach with a MonteCarlo Markov Chain sampler to explore constraints on a ΛCDM model from the shear correlation functions measured in the Canada-France Hawaii Telescope Lensing Survey (CFHTLenS). We obtain constraints on the parameter combination $\sigma_8(\Omega_m/0.27)^{0.6} = 0.801 \pm 0.028$. Combined with results from CMB data, we obtain marginalised constraints on $\sigma_8 = 0.81 \pm 0.01$ and $\Omega_m = 0.29 \pm 0.01$. These results are fully compatible with previous analyses, which supports the validity of our approach. We discuss the advantages of our method and the potential it offers, including a path to incorporate in detail the effects of baryons, among others effects, in future high-precision cosmological analyses.

Key words: gravitational lensing: weak – large-scale structure of the Universe – cosmological parameters – cosmology: observations – cosmology: theory – methods: numerical

1 INTRODUCTION

Gravitational lensing represents a great opportunity to explore fundamental properties of our Universe, e.g. its mean matter density, the properties of primordial density fluctuations, and the nature of dark energy (see, e.g., Bartelmann 2010, for a review). Gravitational lensing shear in the images of distant galaxies has been detected in many surveys (early results include Tyson et al. 1990; Wittman et al. 2000; Bacon et al. 2000; Wilson et al. 2001; Refregier et al. 2002), and it has been used to place direct constraints on cosmological parameters (e.g. Hoekstra et al. 2002, 2006; Fu et al. 2008; Schrabback et al. 2010; Semboloni et al. 2011; Jee et al. 2013; Huff et al. 2014).

One of the largest shear surveys carried out so far is the Canada-France Hawaii Telescope Lensing Survey (CFHTLenS, Heymans et al. 2012), which is based on observations of the Canada-France-Hawaii Telescope Legacy[1] (CFHTLS). An analysis of the cosmological implications of the CFHTLenS 2D shear correlation function was presented in Kilbinger et al. (2013). Fu et al. (2014) extended this analysis by incorporating the information from higher-order correlation functions. Kitching et al. (2014) focused on the cosmological constraints from the reconstructed 3D mass distribution.

The amount and accuracy of weak lensing data will be improved dramatically over the next decade. Surveys such as the Dark Energy Survey[2] (DES), J-PAS[3] or Euclid[4] will scan large fractions of the sky with unprecedented detail, and are expected to reduce current uncertainties in the shear measurements by an order of magnitude. The new data will demand a new level of accuracy and sophistication in its analysis.

A crucial ingredient for a cosmological interpretation of shear data is a description of the nonlinear mass distribution in the Universe as a function of the underlying cosmological model. Analytic prescriptions based on perturbation

[1] http://www.cfht.hawaii.edu/Science/CFHLS/

[2] http://www.darkenergysurvey.org
[3] http://j-pas.org
[4] http://sci.esa.int/euclid

theory break down at the relevant scales, thus N-body simulations are the most accurate way of providing such information (see Kuhlen et al. 2012, for a recent review). Unfortunately, it is currently impossible computationally to carry out thousands of simulations, as it would be required for such analysis. Thus, cosmic shear analyses have mostly relied on fitting functions (e.g. Peacock & Dodds 1996) and/or the halo model (e.g. Seljak 2000; Smith et al. 2003), even though these approaches exhibited noticeable accuracy problems (White & Vale 2004; Hilbert et al. 2009; Sato et al. 2009). Schemes known as emulators (Habib et al. 2007; Heitmann et al. 2010; Schneider et al. 2011), which interpolate between a set of simulations in different cosmologies, have also been proposed, but their application has been hampered by their limited coverage of cosmological parameter space, nonlinear scales and redshift range (Kilbinger et al. 2013). There is a large on-going effort by the community aimed at improving the accuracy and scope of these approaches (see, e.g., Takahashi et al. 2012; Heitmann et al. 2014; Agarwal et al. 2014).

In this paper we explore another way of modelling shear correlation functions, which, we argue, provides a sufficiently flexible and precise theoretical framework for analysing upcoming weak lensing surveys. Our method is based on an extended version of the algorithm originally presented by Angulo & White (2010) (thereafter AW10), which is able to predict the 3D mass distribution – including voids, filaments and self-bound structures – expected in an arbitrary cosmological model. In particular, the method provides predictions for the full hierarchy of mass correlation functions, for halo mass functions and for the cosmic velocity field.

The accuracy of the method is determined by the original N-body simulation employed and by the distance in the cosmological parameter space between the original and target cosmologies. Thus, the associated uncertainty can be controlled by running a small number of N-body simulations with cosmological parameters carefully chosen, and the realism of the predictions is that inherited from the original simulation (which has been steadily increasing over the last 30 years). A great advantage of our method is its full three dimensionality. Since cosmic structures are individually resolved, physically motivated recipes (which can have an explicit dependence on halo mass or assembly history) for how baryons redistribute mass inside halos (e.g. van Daalen et al. 2011, 2014) can be applied. Also, non-trivial survey geometries, selection functions and the source-lens clustering can all be naturally incorporated in the analysis.

These extensions will be described in forthcoming publications. Here we focus on demonstrating that accurate cosmological exploitation is possible using the method. We will show that even with a single cosmology sampled, and with current N-body simulations, it is possible to predict the signal measured by CFHTLenS with an accuracy of $\lesssim 10\%$ (which decreases to $\sim 5\%$ when a smaller range of the cosmological parameter space is considered) and with enough speed to explore almost $100,000$ cosmological models.

The outline of this paper is as follows. In Section 2 we provide the theoretical background for the lensing quantities we will explore. Our model for the shear correlation functions is described in Section 3. Section 4 is devoted to test the performance of our model by comparing its predictions to those from N-body simulations. In Section 5 we present the constraints on cosmological parameters obtained from the CFHTLenS data alone and combined with CMB measurements. Finally, in Section 6 we present our conclusions and discuss future developments of our formalism.

2 THEORY

2.1 Basic definitions

Gravitational lensing, the deflection of light emitted from distant sources by the gravity of matter structures along the line of sight, can shift and shear the images of distant galaxies (e.g. Schneider et al. 2006). The observed image position $\boldsymbol{\theta} = (\theta_1, \theta_2)$ of a source at redshift $z_{\rm S}$ may thus differ from the source's 'true' angular position $\boldsymbol{\beta} = \big(\beta_1(\boldsymbol{\theta}, z_{\rm S}), \beta_2(\boldsymbol{\theta}, z_{\rm S})\big)$. Image distortions caused by differential deflection can be quantified by the distortion matrix

$$\left(\frac{\partial \beta_i(\boldsymbol{\theta}, z_{\rm S})}{\partial \theta_j}\right)_{i,j=1,2} = \begin{pmatrix} 1-\kappa-\gamma_1 & -\gamma_2+\omega \\ -\gamma_2-\omega & 1-\kappa+\gamma_1 \end{pmatrix}, \quad (1)$$

whose decomposition defines the convergence $\kappa(\boldsymbol{\theta}, z_{\rm S})$, the asymmetry $\omega(\boldsymbol{\theta}, z_{\rm S})$, and the complex shear $\gamma(\boldsymbol{\theta}, z_{\rm S}) = \gamma_1(\boldsymbol{\theta}, z_{\rm S}) + {\rm i}\gamma_2(\boldsymbol{\theta}, z_{\rm S})$.

To first order (and to a good approximation in weak lensing); (i) the asymmetry vanishes, (ii) the shear and convergence fields are related through simple phase factors in harmonic space, and (iii) the convergence is given by a weighted projection of the matter density along the line of sight:

$$\kappa(\boldsymbol{\theta}, z_{\rm S}) = \frac{3H_0^2\Omega_{\rm m}}{2{\rm c}^2}\int_0^{\chi_{\rm S}} {\rm d}\chi_{\rm L}\big(1+z_{\rm L}\big)\frac{f_{\rm SL}f_{\rm L}}{f_{\rm S}}\delta_{\rm m}\big(f_{\rm L}\boldsymbol{\theta}, \chi_{\rm L}, z_{\rm L}\big). \quad (2)$$

Here, H_0 denotes the Hubble constant, $\Omega_{\rm m}$ the cosmic mean matter density (in units of the critical density), c the speed of light. We use abbreviations $z_{\rm L} = z(\chi_{\rm L})$, $\chi_{\rm L} = \chi(z_{\rm L})$, $\chi_{\rm S} = \chi(z_{\rm S})$, $f_{\rm L} = f_K(\chi_{\rm L})$, $f_{\rm S} = f_K(\chi_{\rm S})$, and $f_{\rm SL} = f_K(\chi_{\rm S} - \chi_{\rm L})$, where $z(\chi)$ denotes the redshift and $f_K(\chi)$ the comoving angular diameter distance for sources at comoving line-of-sight distance χ, and $f_K(\chi)$ denotes the comoving angular diameter distance for comoving line-of-sight distance χ. Furthermore, $\delta_{\rm m}(f_{\rm L}\boldsymbol{\theta}, \chi_{\rm L}, z_{\rm L})$ denotes the matter density contrast at comoving position $(f_{\rm L}\boldsymbol{\theta}, \chi_{\rm L})$ and redshift $z_{\rm L}$.

2.2 Convergence correlations

For a population of sources with redshift distribution $p_{\rm S}(z_{\rm S})$, an effective convergence can be expressed by

$$\begin{aligned}\kappa(\boldsymbol{\theta}) &= \int {\rm d}z_{\rm S}\, p_{\rm S}(z_{\rm S})\kappa(\boldsymbol{\theta}, z_{\rm S}) \\ &= \int_0^\infty {\rm d}\chi_{\rm L} g(\chi_{\rm L})\delta_{\rm m}\big(f_{\rm L}\boldsymbol{\theta}, \chi_{\rm L}, z_{\rm L}\big),\end{aligned} \quad (3)$$

where $g(\chi_{\rm L})$, the lensing weight factor, is defined as:

$$g(\chi_{\rm L}) = \frac{3H_0^2\Omega_{\rm m}}{2{\rm c}^2}(1+z_{\rm L})f_{\rm L}\int_{z_{\rm L}}^\infty {\rm d}z_{\rm S}\, p_{\rm S}(z_{\rm S})\frac{f_{\rm SL}}{f_{\rm S}}. \quad (4)$$

Assuming a statistically homogeneous and isotropic universe, all two-point correlation functions do not depend on spatial or angular positions, but only on redshift and relative distances. Let angular brackets $\big\langle \ldots \big\rangle$ denote the expectation for an ensemble of universes with a particular set of cosmological parameters. Let

$$\xi(|\boldsymbol{r}|, z, z') \equiv \big\langle \delta_{\rm m}(\boldsymbol{r}', z)\delta_{\rm m}(\boldsymbol{r}'+\boldsymbol{r}, z')\big\rangle \quad (5)$$

denote the two-point correlation function of the matter density contrast. Then, the convergence correlation

$$\xi_\kappa(|\boldsymbol{\theta}|) = \big\langle \kappa(\boldsymbol{\theta}')\kappa(\boldsymbol{\theta}'+\boldsymbol{\theta})\big\rangle \tag{6}$$

can be expressed as

$$\xi_\kappa(\theta) = \int_0^\infty \mathrm{d}\chi_\mathrm{L} \int_0^\infty \mathrm{d}\chi'_\mathrm{L}\, g(\chi_\mathrm{L}) g(\chi'_\mathrm{L}) \times \xi\left(\sqrt{\big(f_\mathrm{L}+f'_\mathrm{L}\big)^2\theta^2/4 + \big(\chi'_\mathrm{L}-\chi_\mathrm{L}\big)^2}, z_\mathrm{L}, z'_\mathrm{L}\right). \tag{7}$$

Define the projected correlation $w(r,z)$ of the density contrast at redshift z and projected comoving separation r by

$$w(r,z) = \int_{-\infty}^\infty \mathrm{d}\chi\, \xi\big(\sqrt{r^2+\chi^2}, z, z\big). \tag{8}$$

Using a Limber-type approximation, the convergence correlation simplifies to

$$\xi_\kappa(\theta) = \int_0^\infty \mathrm{d}\chi_\mathrm{L} g(\chi_\mathrm{L})^2 w\big(f_\mathrm{L}\theta, z_\mathrm{L}\big). \tag{9}$$

2.3 Shear correlations

In cosmic shear surveys, correlations of the shear field are the primary observables. In analogy to the effective convergence, we define an effective shear as:

$$\gamma(\boldsymbol{\theta}) = \int \mathrm{d}z_\mathrm{S}\, p_\mathrm{S}(z_\mathrm{S})\gamma(\boldsymbol{\theta}, z_\mathrm{S}). \tag{10}$$

The shear can be decomposed into a tangential component $\gamma_\mathrm{t}(\boldsymbol{\theta},\boldsymbol{\vartheta})$ and a cross component $\gamma_\times(\boldsymbol{\theta},\boldsymbol{\vartheta})$ with respect to any given direction $\boldsymbol{\vartheta}$ (e.g. Schneider et al. 2002):

$$\gamma_\mathrm{t}(\boldsymbol{\theta},\boldsymbol{\vartheta}) + \mathrm{i}\gamma_\times(\boldsymbol{\theta},\boldsymbol{\vartheta}) = -\mathrm{e}^{-2\mathrm{i}\varphi(\boldsymbol{\vartheta})}\gamma(\boldsymbol{\theta}), \tag{11}$$

where $\varphi(\boldsymbol{\vartheta})$ denotes the polar angle of the vector $\boldsymbol{\vartheta}$. With this decomposition, two translation and rotation invariant shear correlation functions can be defined (e.g. Kaiser 1992):

$$\xi_\pm\big(|\boldsymbol{\theta}|\big) = \big\langle \gamma_\mathrm{t}(\boldsymbol{\theta}',\boldsymbol{\theta})\gamma_\mathrm{t}(\boldsymbol{\theta}'+\boldsymbol{\theta},\boldsymbol{\theta})\big\rangle \pm \big\langle \gamma_\times(\boldsymbol{\theta}',\boldsymbol{\theta})\gamma_\times(\boldsymbol{\theta}'+\boldsymbol{\theta},\boldsymbol{\theta})\big\rangle\,. \tag{12}$$

These cosmic shear correlation functions can be directly estimated from the observed image ellipticity of distant galaxies.

Exploiting the relation between shear and convergence in harmonic space,

$$\xi_+\big(\theta\big) = \xi_\kappa(\theta) \quad \text{and} \tag{13}$$

$$\xi_-\big(\theta\big) = \xi_\kappa(\theta) + \int_0^\theta \mathrm{d}\theta' \left(\frac{4\theta'}{\theta^2} - \frac{12\theta'^3}{\theta^4}\right)\xi_\kappa(\theta'). \tag{14}$$

Thus, by defining

$$w_+(R,z) = w(R,z) \quad \text{and} \tag{15}$$

$$w_-(R,z) = w(R,z) + \int_0^R \mathrm{d}R' \left(\frac{4R'}{R^2} - \frac{12R'^3}{R^4}\right) w(R',z), \tag{16}$$

we can write the shear correlations as

$$\xi_\pm(\boldsymbol{\theta}) = \int_0^\infty \mathrm{d}\chi_\mathrm{L} g(\chi_\mathrm{L})^2 w_\pm\big(f_\mathrm{L}\theta, z_\mathrm{L}\big). \tag{17}$$

Therefore, observational measurements of shear correlations encode information about the statistical properties of the mass in the Universe at different cosmic epochs.

3 DATA

3.1 Shear correlation functions from CFHTLenS

We use the measurements of cosmic shear correlation functions, $\xi_\pm$ (c.f. Eq. 12), by Kilbinger et al. (2013) from the Canada-France-Hawaii Telescope Lensing Survey (CFHTLenS, Heymans et al. 2012). CFHTLenS is based on observations of the Canada-France-Hawaii Telescope Legacy (CFHTLS), and it currently offers one of the most informative astronomical datasets for cosmic shear. The survey spans 154 square degrees observed in five optical bands u^*, g', r', i', and z' with a 5σ point-source apparent magnitude limit $i'_{AB} \sim 25.5$. The CFHTLenS analysis combines weak lensing data processing with THELI (Erben et al. 2013), shear measurement with lensfit (Miller et al. 2013), and photometric redshift measurement with PSF-matched photometry (Hildebrandt et al. 2012). A full systematic error analysis of the shear measurements in combination with the photometric redshifts is presented in Heymans et al. (2012), with additional error analyses of the photometric redshift measurements presented in Benjamin et al. (2013).

Kilbinger et al. (2013) used approx. 75% of the full CFHTLS area (selected according to results from tests for residual systematic errors) to measure shear correlation functions $\xi_\pm(\theta)$ on scales $0.9\,\mathrm{arcmin} \leqslant \theta \leqslant 300\,\mathrm{arcmin}$. The background galaxies for the shear correlation measurements have a mean number density $\bar{n} \sim 17\,\mathrm{arcmin}^{-2}$ and mean redshift $\bar{z} \sim 0.75$. In this paper we will employ the publicly-available source redshift distribution, measured shear correlations, and data covariance[5].

3.2 Cosmic Microwave Background measurements

We combine our cosmological constraints from the shear data with those derived from Cosmic Microwave Background (CMB) measurements, which will help to break degeneracies among cosmological parameters. Specifically, we use a combination of the CMB temperature power spectrum from the 1st year data of the Planck satellite (Planck Collaboration et al. 2013), CMB temperature measurements on small angular scales from the Atacama Cosmology Telescope (ACT, Das et al. 2014) and the South Pole Telescope (SPT, Story et al. 2013), and polarization measurements on large scales (low multipoles) from the Wilkinson Microwave Anisotropy Probe (WMAP, Hinshaw et al. 2013). For simplicity we refer to this combination as "Planck".

4 METHODOLOGY

In this section we describe our model for the shear correlation expected from a given lensing survey. In §4.1 we describe an improved version of the algorithm proposed by Angulo & White (2010), which we use together with the N-body simulations described in §4.2 to predict the projected mass correlation functions in an arbitrary cosmology. In §4.4 we describe how these can be combined to compute shear correlation functions.

[5] `http://www.cfhtlens.org`

4.1 Rescaling mass correlations functions

The first and most important ingredient to exploit shear observations is predictions for the nonlinear mass correlation function as a function of redshift for an arbitrary cosmological model. This is often given by fitting functions, emulators or analytic prescriptions based on the halo model. Here, we adopt a different path, exploiting the method of AW10, which alters the length, mass and time units of an N-body simulation to mimic the three-dimensional mass distribution of an N-body simulation carried out for a different set of cosmological parameters.

We refer to the original AW10 paper for details of the method, and to Ruiz et al. (2011) and Mead & Peacock (2014) for additional tests. Here, we simply recall that the method is able to rescale the mass distribution of a simulation such that matter and halo power spectra are matched to better than 5% at all redshifts (and $\lesssim 2\%$ deviation at $z = 1$), over the whole range of scales tested, i.e. 1 to 500 Mpc. In addition, the mass function of DM halos is reproduced with an error $\lesssim 10\%$.

Although the accuracy of the method of AW10 is already high, here we have modified it slightly to enhance its performance. In the original formulation of the method, the rescaling parameters are set by a match between the variance of the linear mass field in the rescaled and target cosmologies. Here, we seek the best scaling parameters by also requiring that the growth history be as close as possible between the rescaled and target simulations.

Explicitly, we compute the linear growth history for scaled cosmologies within $\Delta \log a_* = 0.1$, where a_* is the expansion factor in the original cosmology that best represents the $a = 1$ output in the target cosmology. Then, we select as a new scaled cosmology that with the closest growth history to that of the target cosmology. We do this by comparing 10 expansion factor values (uniformly-spaced between $a = 0.1$ and 1). We note that the weight given to matching the growth and the linear variance is, at the moment, empirical. However, in principle it is possible to adapt the weight for each target cosmology in order to minimize a suitably defined global uncertainty.

This modification aims at taking into account the assembly history of dark matter halos, which is expected to largely determine the density profile of halos (Ludlow et al. 2013b,a). Thus, this is expected to increase the accuracy of the AW10 method on small scales. In §5.3 we will present a comparison of the original and modified AW10 algorithm applied to predict CFHTLenS shear correlations.

The final step in the AW10 algorithm is to perform a quasi-linear distortion of the 3D mass distribution that accounts for differences in the shape of the primordial power spectrum between the scaled and target cosmologies. We will refer to this as large-scale structure correction.

The algorithm described in this section opens the remarkable option of creating 3D maps for the expected mass distribution in any cosmology. We simply need an N-body simulation with enough volume, mass and time resolution to match the requirements placed by the dataset to be modelled. In the next section we describe a suite of simulations that meets these requirements for analysing the CFHTLenS data.

4.2 N-body simulations

Our analysis uses the projected mass correlation functions measured in the Millennium Simulation (MS) suite: MS-I (Springel et al. 2005), MS-II (Boylan-Kolchin et al. 2011) and MXXL (Angulo et al. 2012). The MS runs adopt a matter density of $\Omega_{\rm m} = 0.25$ in units of the critical density, a cosmological constant with $\Omega_\Lambda = 0.75$, a Hubble constant $h = 0.73$ in units of $100\,{\rm km\,s^{-1}Mpc^{-1}}$, a spectral index $n_s = 1$ and a normalisation parameter $\sigma_8 = 0.9$ for the primordial linear density power spectrum. In Table 1 we summarize the box size, particle mass and the Plummer-equivalent gravitational force softening employed in each run of the MS suite.

Table 1. Properties of the simulations used in this work. $\rm N_p$ is the number of particles; $L_{\rm box}$ is the box size of the simulation; ϵ is softening length and $m_{\rm p}$ is the particles mass.

Simulation	N_p	$L_{\rm box}$ [Mpc/h]	ϵ [kpc/h]	$m_{\rm p}$ [$\rm M_\odot/$$h$]
MS-XXL	6720^3	3000	10	6.17×10^9
MS-I	2160^3	500	5	8.61×10^8
MS-II	2160^3	100	1	6.89×10^6
Test-Small	1080^3	250	5	$8.61\times10^8\,\left(\frac{\Omega_{\rm m}}{0.25}\right)^{1/3}$
Test-Large	512^3	1500	60	$1.75\times10^{11}\,\left(\frac{\Omega_{\rm m}}{0.25}\right)^{1/3}$

The cosmological parameters of the MS are different to those preferred by recent analyses, in particular, the value of σ_8 is about 10% higher than current best fit values (e.g. Planck Collaboration et al. 2013). This is, however, an advantage for our analysis since higher fluctuation amplitudes allow the MS to be scaled to a wider range of cosmologies. To further increase the scalable region of the parameter space, we have evolved the full MS-I beyond $z = 0$, until $z = -0.846$ (or, equivalently to an expansion factor of 6.5) using the memory efficient version of the `L-Gadget3` code described in Angulo et al. (2012). We store 20 additional snapshots, roughly equally spaced in linear growth factor. This allow us to predict the cosmic structure in, for instance, a cosmology with a value of σ_8 equal to 1.1.

4.3 Projected correlation functions

At each output time, we compute the projected correlation function of the mass distribution as follows:

$$w(r,z) = 2\int_{x_{\rm min}}^{x_{\rm max}} {\rm d}x\,\xi\big(\sqrt{x^2+r^2},z\big) \qquad (18)$$

where $\xi(r,z)$ denotes the 3D correlation function at separation r of the matter density contrast at redshift z. We compute ξ in Fourier space employing a 4096^3 grid, following the procedure described in Angulo et al. (2013). We repeat the calculation twice after folding the box size 8 times in each direction, which allows us to compute $\xi(r)$ on much smaller scales: for the MS-I this scale is $r_{\rm min} = 500/8/8/4096 = 2\,{\rm kpc}/h$. In the case of the MXXL, only the density field on a 2048^3 grid was stored at every output, so we use these when computing the correlation function. We set $x_{\rm min} = 10^{-4}\,{\rm Mpc}/h$ and $x_{\rm max} = 100\,{\rm Mpc}/h$. We also set $\xi(r) = \xi(r_{\rm min})$ for all $r < r_{\rm min}$, since $x_{\rm min} < r_{\rm min}$.

For testing the correctness and accuracy of our calculations, we also compute the projected correlations in a different way: For each simulation output, the matter distribution is first projected onto the simulation box faces. Then the correlation of the projected matter densities is computed using a 2D Fast Fourier method. To compute the correlations on large

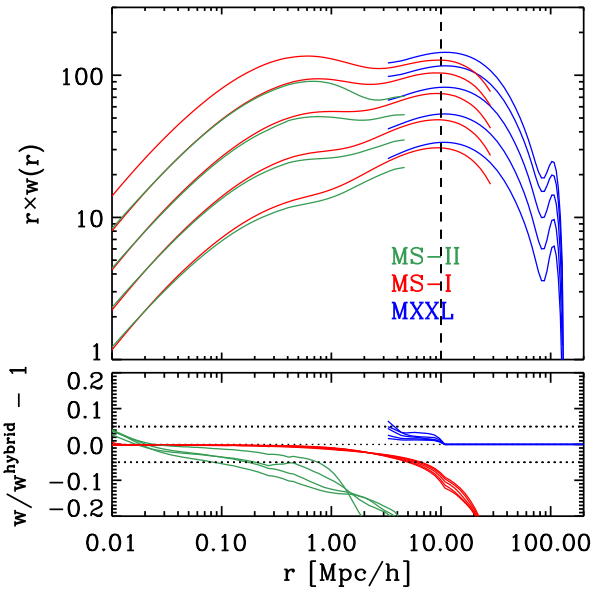

Figure 1. The projected mass correlation function, $w(r)$, measured in the Millennium Simulations suite, at 5 different output times. From bottom to top these are $z = 1.5$, 0.9, 0.4, 0.0, and -0.25. For each redshift, coloured lines show results for the MS-II (green), MS (red) and MXXL (blue) runs, as indicated by the figure legend. Note we display $r \times w(r)$ to enhance the effective range shown.

scales, coarse meshes covering the whole box faces are used. For the correlation on smaller scales, the box faces are tiled with a set of smaller but finer meshes, on which the correlations are computed using appropriate zero-padding to account for non-periodic boundary conditions (Hilbert et al. 2011). A comparison of the results from this approach to the first approach based on 3D correlations shows a good agreement. For scales $r < 50\,\mathrm{Mpc}/h$, both estimates agree at the 3% level for the $z = 0$ output of the MXXL simulation. On larger scales, cosmic variance dominates the correlation function of the projected mass field.

The identical output times and cosmological parameters of the MS runs enable a detailed comparison as well as a joint use of these simulations. In Fig. 1 we show the projected correlation functions measured in the three MS at 5 output times: $z = 1.5$, 0.9, 0.4, 0.0, and -0.25, from bottom to top. By comparing the three simulations we can clearly see the effects of force resolution and box size, both of which decrease the amplitude of the projected correlation function. The finite box size and lack of long wavelengths have a greater impact on the projected correlations than on spherically averaged correlation functions. The finite-volume effect is found 10% at a scale of 1/50 of the box size, roughly independent on redshift, which is in good agreement with analytical estimates. The effect of the force resolution also appears to be redshift independent and of a magnitude of 10% at a scale twice as large as the softening length ($5\,\mathrm{kpc}/h$ in the MS-I).

We see that none of the simulations individually can predict the projected correlation function accurately, thus, we have built a hybrid correlation function, $\xi^{\rm hybrid}$, by combining the results of the MXXL on scales larger than $r_{\rm t} = 7\mathrm{Mpc}/h$, and those of the MS-I on smaller scales. Explicitly:

$$\xi^{\rm hybrid}(r,z) = \xi^{\rm MS-I}(r,z)\,\mathrm{erfc}\left(\frac{r-r_{\rm t}}{2.5}\right)/2 + \quad (19)$$

$$\xi^{\rm MXXL}(r,z)\left[1-\frac{1}{2}\mathrm{erfc}\left(\frac{r-r_{\rm t}}{2.5}\right)\right] \quad (20)$$

For $z < 0$, we use the MS-I evolved into the future (c.f. §4.2) and the $z = 0$ MXXL measurement linearly scaled to the appropriate (negative) redshift. Although not shown here, we note that, at the transition scale ($7\,\mathrm{Mpc}/h$), the measurements from the MS-I and MS-XXL agree at the $2-3$% level, over all redshifts examined. At this point, we refrain from using the MS-II, since the MS-I is sufficient to model the smallest scales relevant for our purposes.

The bottom panel of Fig. 1 shows the fractional differences of the projected correlations of the individual simulations relative to the hybrid result. At all redshifts, we can see that our combined model employs different simulations where they are most accurate, resulting in an accuracy of 5% or better. We use these combined correlations together with the scaling method described above for the remainder of this paper. However, we note that future simulations with higher force resolution and larger volumes should provide an even more accurate starting point for our formalism.

4.4 Modelling the shear correlation function measurements

After computing the hybrid projected correlation functions described in above, we find the scaling parameters for a given target cosmological model. Then we change the length unit of the projected correlation functions accordingly, and re-associate each output with a different cosmic time.

For computing the shear correlations, we first partition the lightcone into intervals $\mathbb{I}^{(k)} = \left[\chi^{(k)}_{\rm L,hi}, \chi^{(k)}_{\rm L,lo}\right)$, $k = 1, \ldots, N_{\mathbb{I}}$ that match the scaled output times of our N-body results. Within each $\mathbb{I}^{(k)}$, we select a point $\chi^{(k)}_{\rm L} \in \mathbb{I}^{(k)}$ by choosing the comoving line-of-sight distance to the scaled snapshot time in the target cosmology. Then, we split the integral (17) into integrals over the intervals, and approximate the integrands by their mid values:

$$\begin{aligned}\xi_\pm(\boldsymbol{\theta}) &= \sum_k \int_{\chi^{(k)}_{\rm L,hi}}^{\chi^{(k)}_{\rm L,lo}} \mathrm{d}\chi_{\rm L}\, g\big(\chi_{\rm L}\big)^2 w_\pm\big(f_{\rm L}\theta, z_{\rm L}\big) \\ &\approx \sum_k \left(\chi^{(k)}_{\rm L,lo} - \chi^{(k)}_{\rm L,hi}\right) g\big(\chi^{(k)}_{\rm L}\big)^2 w_\pm\big(f^{(k)}_{\rm L}\theta, z^{(k)}_{\rm L}\big).\end{aligned} \quad (21)$$

The discretisation allows us to compute the shear correlations from the matter correlations at a finite number of redshifts, in particular those of snapshot outputs of a given simulation. This approximation becomes inaccurate if the simulation output times sample the matter evolution to sparsely. Discretisation accuracy tests will be discussed in §5.2.

As an alternative to the sum (21), one may obtain a better approximation by using the matter correlations of the snapshots to construct an interpolation of the matter correlation as function of scale and redshift, and then feeding that interpolation function into the integral. Here, we will not pursue this option since, as discussed later, our model already appears accurate enough to exploit the CFHTLenS measurements.

In this work, we use a source galaxy redshift distribution that is given as galaxy numbers $n_{{\rm S},i}$ at a number of discrete source refshifts $z_{{\rm S},i}$ (i.e. as a source redshift histogram). In

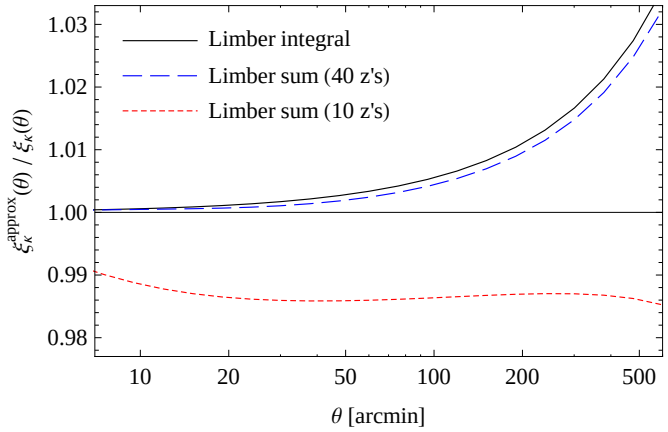

Figure 2. Systematic error on the computed convergence correlation $\xi_\kappa(\boldsymbol{\theta})$ to sources at redshift $z = 0.75$ as a function of pair separation $\boldsymbol{\theta}$ due to Limber-type approximations. Shown is the ratio of the approximated expression and the full expression (7) for the Limber integral (9) (black solid line), and for its discretisation (21) using either 40 (blue dashed line) or just 10 redshifts (red dotted line).

that case, the lensing weight factors (4) can be expressed as sums, too,

$$g(\chi_{\rm L}) = \frac{3H_0^2\Omega_{\rm m}}{2c^2}(1+z_{\rm L})f_K\chi_{\rm L}\sum_i n_{{\rm S},i}\frac{f_K(\chi_{{\rm S},i}-\chi_{\rm L})}{f_K(\chi_{{\rm S},i})}. \qquad (22)$$

5 TESTS

We now test the methodology presented in the previous section. We start by comparing our predictions for shear correlation functions using the discretised integrals to the predictions from the continuous Limber and full integrals (§5.1). Next, we compare our predictions to results from full ray-tracing (§5.2). We then asses the performance of the cosmology-scaling method by carrying out direct N-body simulations covering a wide range of target cosmologies (§5.3).

5.1 Limber approximation and discretised integrals

The predictions in our approach are based on a Limber-type approximation (9) for the convergence correlation, and further discretisation (21) of the resulting integral. To estimate the effect of these approximations, we first model the matter density correlation by a simple fit to the measured correlation:

$$\xi(r,z,z') = \frac{1}{1+r^2/r_{\rm s}^2}\frac{1}{1+r^2/r_{\rm c}^2}\exp\left(-\frac{\chi(z)+\chi(z')}{\chi_{\rm c}}\right). \qquad (23)$$

With the parameters $r_{\rm s} = 0.1h^{-1}$Mpc, $r_{\rm c} = 100h^{-1}$Mpc, and $\chi_{\rm c} = 3200h^{-1}$Mpc, the fit captures the scale and redshift dependence of the correlation well enough for our purposes. We then use this fit as input matter correlation in the expressions (7), (9) and (21) for the convergence correlations.

The results of this test are illustrated in Fig. 2. The errors introduced by the Limber approximation are well below 1% for separations $\theta < 3$ deg. And even for scales $\theta \sim 5$ deg, the errors stay below 5%. The discretisation errors are very small (and of opposite sign to the Limber approximation error), too, e.g. $1-5\%$ even if only ~ 10 redshifts are used in the sum (for the more typical 40 redshifts, the error is much smaller).

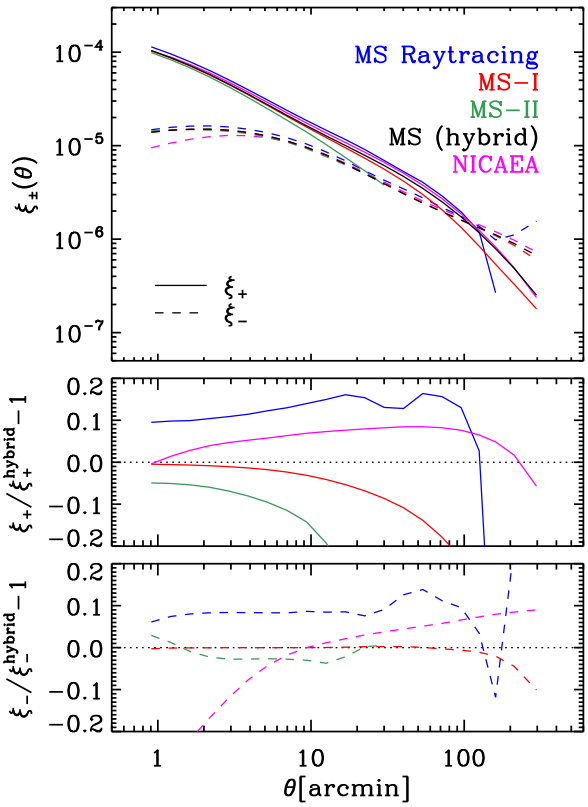

Figure 3. Comparison of the shear correlation functions predicted by several methods: a full ray-tracing algorithm applied to the MS-I simulation (blue lines), a halo-model as implemented by the `NICAEA` code (magenta lines), a discretised integrals (c.f. Eq. 18) employing a hybrid correlation function (our preferred model, black lines), or those measured directly in the MS-I simulation (red lines) or MS-II (green lines). The middle and bottom panels show the fractional differences with respect to our preferred model for ξ_+ and ξ_-, respectively.

5.2 Discretised integrals versus ray-tracing simulations

In Fig. 3, we present a comparison of the CFHTLenS shear correlation functions predicted for the MS cosmology by (i) a full ray-tracing simulation performed on the MS-I (blue lines), (ii) a commonly used method based on the halo model (magenta lines), and (iii) the algorithm described in the previous section. For the latter we display cases where the input mass correlation function was computed from the MS (red lines), the MS-II (green lines), and our fiducial model based on the hybrid correlation functions (black lines) described in §4.3. In the middle and bottom panels, we show fractional differences of these models with respect to this hybrid one. In all cases, we employ the redshift distribution of background galaxies provided by the CFHTLenS collaboration.

Firstly, it is clear that the MS-I and MS-II simulation boxes are not big enough to accurately describe correlations on scales larger than ~ 30 and 3 arcmin, respectively. As it was also shown in Fig. 1, the lack of long-wave modes reduces the amount of correlation on large scales. This highlights the need of the MXXL simulation for our analysis, and for a correct interpretation of shear signals. By comparing our hybrid

model with the predictions of the MS-II simulation, we can see that the much higher force resolution of the latter simulation is important only at the 5% level and for the smallest scales, which justifies our choice of not including it in our hybrid predictions. We note that these scales might also be contaminated by baryonic effects, which we do not attempt to model here.

We now compare our predictions with the results of the ray-tracing algorithm (blue lines) described in Hilbert et al. (2009). In brief, this method constructs multiple-lens-plane lightcones from the MS outputs, and then traces light rays backward through this series of lens planes, computing light deflections at the lens planes from the projected matter distribution on these planes. We show correlation functions estimated from 64 ray-traced fields of $4\times4\,\mathrm{deg}^2$. Error bars display the standard deviation over them. We note that multiple realisations are needed to perform a more accurate comparison: Since the ray-tracing procedure involves a light-cone construction, the predictions are more affected by cosmic variance than our discretised integrals (which use the full simulation box at each output time, instead of a small cone segment).

We can see that these results agree reasonably well with our (comparatively) very simplified treatment of gravitational lensing effects. This supports the validity of our approximations and implementation. There is, however, a systematic excess in the ray-tracing correlations of about $10-15\%$ for both ξ_+ and ξ_- with respect to our model. The discrepancy increases to about a factor of two when compared to the MS-I based predictions on large scales. We have investigated several possible sources for the discrepancy. However, we have found none apart from cosmic variance that could plausibly explain this finding.[6] Since this systematic variation is not significant compared to the uncertainty in the CFHTLenS data, we postpone a deeper exploration of this issue to a future publication.

Finally, we compare our method with predictions based on the halo model – one of the most popular models employed in the literature. In particular, magenta lines display the predictions of the implementation in NICAEA (Kilbinger et al. 2012). Similarly to the ray-tracing case, we find a reasonably good agreement with our model, with a discrepancy of $< 10\%$ for ξ_+. This model, however, performs poorly on small scales for ξ_-, where underestimates the signal by a factor of 2, with respect to the raytracing results and those of our model. We note that recent improvements to the halo model (e.g. Takahashi et al. 2012) should produce more accurate predictions.

5.3 Cosmology scaling versus direct N-body simulations

We now probe the accuracy of the scaling method described in §4.1 in predicting $\xi_\pm$ as a function of cosmology. For this, we have carried out 6 N-body simulations employing different combinations for Ω_m and σ_8. Specifically, we use: $(\Omega_m,\sigma_8) = (0.15,1.1)$, $(0.15,1.0)$, $(0.25,0.5)$, $(0.5,0.7)$, $(0.8,0.4)$, $(0.29,0.81)$, which were chosen to approximately cover the whole region of the parameter space we will explore. For each cosmology we have run two different simulation boxes, $L_{\rm box} = 250\,\mathrm{Mpc}/h$ and $1500\,\mathrm{Mpc}/h$, referred to as Test-Small and Test-Big. The numerical parameters of these simulations are given in Table 1. We highlight that the output structure is identical to those of the MS, and that the mass and force resolution of the Test-Small suite matches that of the MS-I run. In an analogous manner to the construction of our fiducial model, we combine the measured correlation functions of the Test-Small and Test-Big simulation suites to accurately cover the whole relevant range of scales.

Fig. 4 shows one of the main results of this paper: a comparison of the shear correlation functions predicted from direct simulations and from our algorithm. In all cases, our procedure correctly captures the dependence of $\xi_\pm$ on cosmology. The agreement between the direct and scaled predictions is remarkable, and in several cases and scales, both predictions are indistinguishable by eye! The precision is particularly high for ξ_+ where differences are always smaller than 10%, and somewhat lower for ξ_-, specially on small angular scales where the differences can reach up to 17%. We emphasise that we are considering very extreme cosmologies. When we focus on a cosmology compatible with the latest Planck results (bottom right panel), the differences are $< 3-4\%$ for both ξ_+ and ξ_-.

We have a closer look at the error in our procedure in Fig. 5, where we display the fractional uncertainty introduced by our scaling procedure. Specifically, we plot $\xi_\pm^{\rm scaled}/\xi_\pm^{\rm N-body} - 1$, where $\xi_\pm^{\rm scaled}$ is one of three cases: our cosmology-scaling algorithm with and without the large-scale correction (green and red lines, respectively), and the original AW10 without the large-scale correction (blue lines).

Firstly, we note that there is a pattern in the sign of the deviations for all three methods. Cosmologies that require a length scaling larger than the unity have positive deviations, whereas those with a scaling scaling smaller than unity have negative deviations. As the smallest angular scales predicted by the MS are affected by its limited force resolution, this suggests that force resolution is responsible for at least some of the discrepancy on small scales shown in Fig. 5.

By comparing red and blue lines we can see that, for all cosmologies, our modified AW10 method performs better than the original one on small scales, in some cases reducing the error by a factor of 2 and confirming our expectations set in § 4.1. More similar growth histories imply more similar formation times and concentration-mass relation, which in turn impacts positively the accuracy of the scaled correlation functions on small scales. On larger scales, the original method performs better. As it does not have the additional constraint of matching growth histories, it is a better fit to the overall shape of the linear theory power spectrum. Nevertheless, this is in principle not important since the large-scale correction brings back the high accuracy of the method at all scales.

It is also clear that the larger the difference in cosmological parameters, the less accurate the scaled predictions are. Below 100 arcmin, for ξ_+, the largest fractional difference is found for the $(0.5,0.7)$ cosmology. Due to the high value of Ω_m, this simulation does not feature a slow down of structure formation caused by a cosmological constant, as it is the case for the MS cosmology. On the other hand, the $(0.81,0.29)$ cosmology shows the smallest fractional difference; it has a similar power spectrum and growth history as the MS. This is an interesting feature since it opens up the possibility of suitably defining locations in the cosmological parameter space for performing direct N-body simulations designed to be scaled. Such an ensemble of simulations can then ensure a given accuracy of scaled shear correlations.

As we have seen here (and also discussed in AW10), the large-scale correction is an important aspect of the method. Unfortunately, the computational cost associated is too high

[6] The Limber approximation, for example, causes errors $\lesssim 1\%$ on the scales of interest.

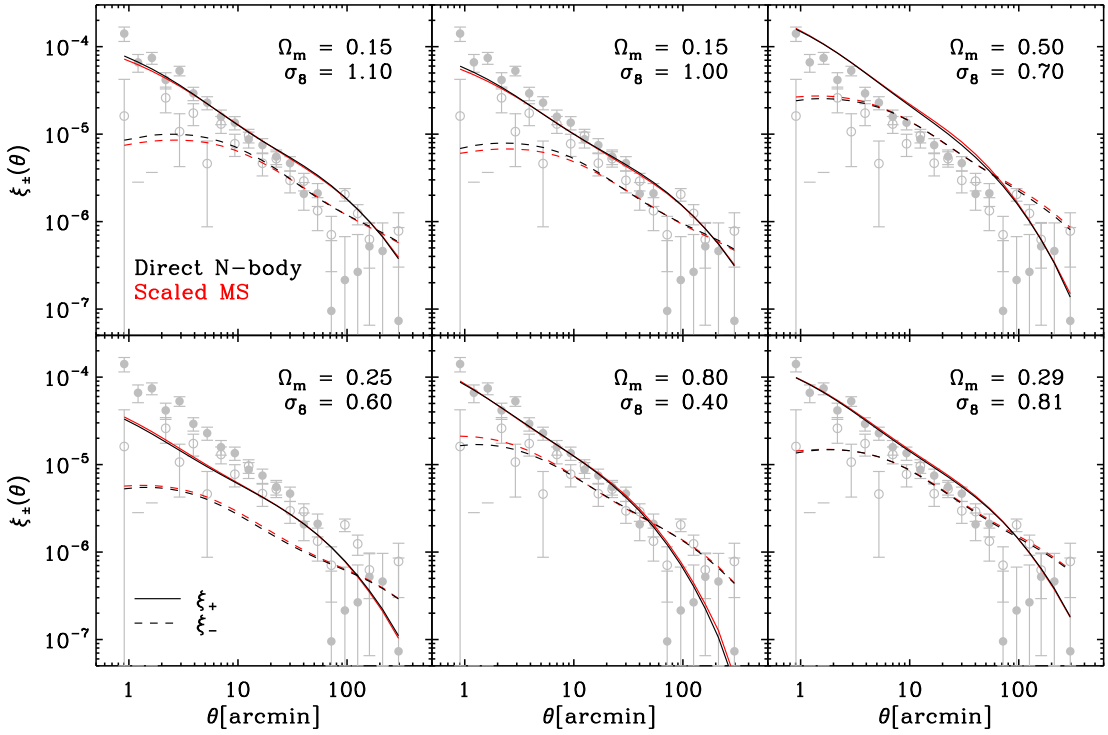

Figure 4. Comparison between the predictions of the theoretical model described in §4.1 (red lines) and direct N-body simulations (black lines, see §4.2). Each subpanel displays results for $\xi_+(\theta)$ (solid lines) and $\xi_-(\theta)$ (dashed lines) for a different combination of $\Omega_{\rm m}$ and σ_8, as indicated by the figure legends. CFHTLenS measurements together with their uncertainty (grey symbols and error bars) are shown for comparison.

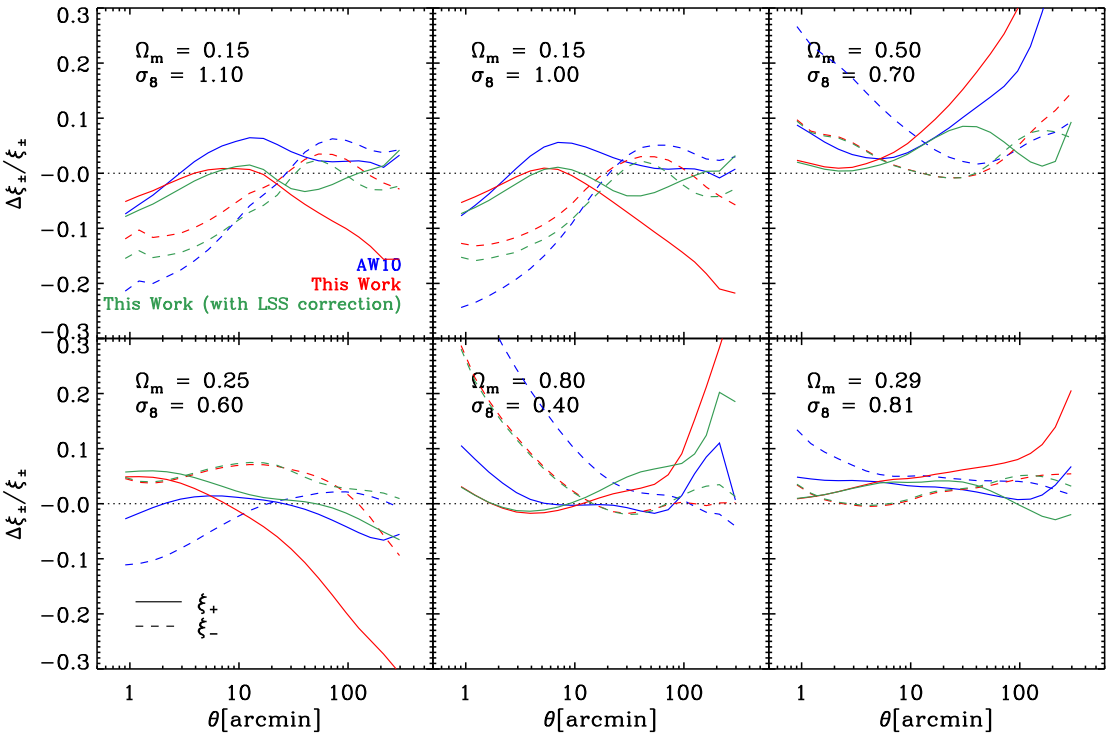

Figure 5. Fractional difference between the shear correlation functions, $\xi_\pm$, predicted by direct N-body simulations and three slightly different cosmology scaling methods.

for it to be used in an exploration of a cosmological parameter space. Although it is possible to perform a fast large-scale correction directly on the measured correlations using low-pass-filtered linear-theory correlation functions, at all scales and for all cosmologies, even the methods without this correction have a small associated systematic error: They range from 20 to 60% of the square root of the diagonal elements of the data covariance matrix at the respective scale. This implies that the cosmology scaling without the large-scale correction is indeed accurate enough for the exploitation of CFHTLenS data, and thus, we will use this for the remainder of our paper. We note we choose our modified AW10 scheme over the original one because large angular scales in the data show the largest variance. Thus, relative to the uncertainties in the measurements, accuracy on large scales are less important than that on smaller angular scales.

To summarize this section, we conclude that the algorithm proposed and developed here is of high accuracy for the cosmological exploitation of the CFHTLenS data. At each point of the parameter space would be possible to quickly predict the full three-dimensional and nonlinear structures expected in any cosmological model, together with the expected lensing shear they produce.

6 COSMOLOGICAL CONSTRAINTS

We now apply the new algorithm presented and tested in previous sections to obtain cosmological constraints from the CFHTLenS data. In §6.1 we discuss the cosmological parameters to be explored, and also describe the method used to sample their probability distribution function. In §6.2 we present and discuss the cosmological implications of our analysis.

6.1 Parameter Space and Likelihood calculation

In this paper we explore the parameters of the minimal ΛCDM model, where we assume Gaussian and adiabatic primordial fluctuations, a flat space geometry, a dark energy component in the form of a cosmological constant, and a negligible contribution of massive neutrinos and tensor perturbations. This simple model is specified by 5 parameters:

$$\boldsymbol{\pi} = (\sigma_8, \Omega_m, \Omega_b, n_s, h), \tag{24}$$

the *rms* linear density fluctuations in spheres of radius 8Mpc, σ_8; the total mass density in units of the critical density, $\Omega_m = \Omega_{\rm dm} + \Omega_b$, where Ω_b and $\Omega_{\rm dm}$ refer to baryons and dark matter, respectively; the primordial spectral index, n_s; and the present-day Hubble constant, in units of $100\,{\rm km\,s^{-1}\,Mpc^{-1}}$. The priors for these parameters are assumed to be flat and over the range: $\sigma_8 \in [0.4, 1.1]$, $\Omega_m \in [0.1, 0.8]$, $\Omega_b \in [0, 0.1]$, $n_s \in [0.7, 1.2]$ and $h \in [0.4, 1.0]$.

We assume that the probability of observing a given set of cosmic shear values $\boldsymbol{\xi} = \left(\xi_+(\vartheta_1), \ldots\right)$ is given by a multivariate normal distribution

$$p(\boldsymbol{\xi}|\boldsymbol{\pi}) \propto \exp\left\{-\frac{1}{2}[\boldsymbol{\xi} - \boldsymbol{m}(\boldsymbol{\pi})]^{\rm t}\,\Sigma_{\rm d}^{-1}\,[\boldsymbol{\xi} - \boldsymbol{m}(\boldsymbol{\pi})]\right\}. \tag{25}$$

Here, $\Sigma_{\rm d}$ is the data covariance matrix as computed by Kilbinger et al. (2013) for the CFHTLenS shear correlation functions. $\boldsymbol{m}(\boldsymbol{\pi})$ denotes the expected cosmic shear signal computed with our model described in §4. We recall that this model shows an accuracy better than 10% over the whole range of scales explored even for very extreme cosmologies and without any nuisance parameters. When considering target cosmologies closer to the best fit values of the ΛCDM model, the accuracy of our model increases to the few percent level.

In our model we neglect the effects induced by "baryonic physics", which can redistribute mass inside halos through gas cooling and feedback from star formation, supernovea, and AGNs possibly affecting the shear signal (e.g. Semboloni et al. 2011; Zentner et al. 2013). However, as shown by Kilbinger et al. (2013), excluding small scales ($\theta < 17$ arcmin or $\theta < 53$ arcmin) does not significantly shift the cosmological constraints derived, which suggests that the effect is statistically unimportant given the accuracy of the CFHTLenS measurements.

Nevertheless, we note that due to the 3D nature of our models, where individual halos are resolved for each target cosmological model, such effect could in principle be parametrized and incorporated into our formalism. The additional uncertainty can be naturally marginalised over, providing robust cosmological constraints. Carrying out such analysis, although possible, is still a tough computational challenge. However, continuous development in algorithms and supercomputing power make us optimistic about a successful outcome in the near future.

We sample the posterior probability using our own implementation of the Markov Chain Monte Carlo algorithm (MCMC). At each step of the chain, we use CAMB (Lewis et al. 2000) to compute the linear theory mass fluctuations power spectrum for the target cosmological parameter vector. This power spectrum together with the expected growth history are then used to compute the best scaling parameters, which in turn are used together with the precomputed projected correlation functions to predict the shear correlation functions expected in the target cosmological scenario. We repeat this procedure for 8 independent chains with $10,000$ steps each and a burning phase of 200 steps.

To make the analysis feasible, we heavily optimised all numerical codes involved. As a result, each step in the chain can be carried out in less than 4 seconds, including the linear-theory calculation and the cosmology-rescaling algorithm.

6.2 Cosmological constraints

We now present the constraints estimated from the CFHTLenS data. We focus on the parameters σ_8 and $\Omega_{\rm m}$, as these contain most of the cosmological information encoded in the shear correlation functions. The constraints on the other 3 parameters of our model are rather weak.

Fig. 6 shows the two-dimensional marginalised constraints in the $\Omega_{\rm m}$-σ_8 plane obtained from applying our model to the measured shear correlation functions. The red and orange regions denote the 68 and 96 per cent confidence levels.

The constraints are elongated along the degeneracy that approximately corresponds to a constant value of $\sigma_8^{-1}\Omega_{\rm m}^{0.6}$. This is a result of a combination of geometrical and growth effects. Our best-fit value for this parameter combination is $\sigma_8^{-1}\Omega_{\rm m}^{0.6} = 0.801 \pm 0.028$, which is displayed as a long dashed line in Fig. 6.

For comparison, the result of Kilbinger et al. (2013) is displayed as a dotted line. These authors find $\sigma_8^{-1}\Omega_{\rm m}^{0.6} = 0.79 \pm 0.03$ using the same dataset and a theoretical model based on

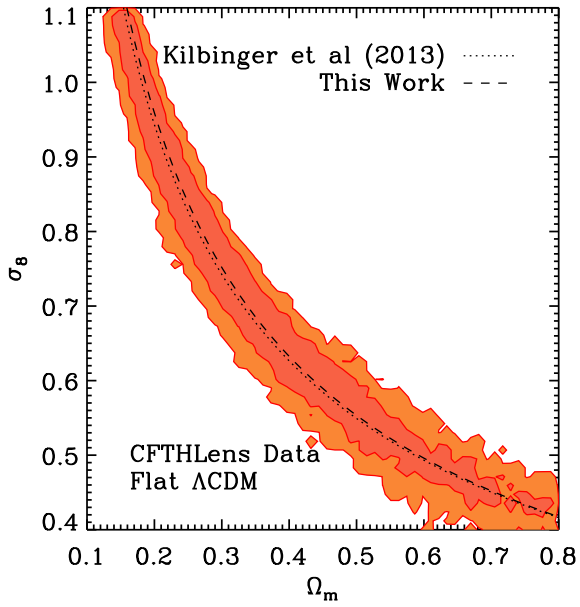

Figure 6. Marginalised 68% and 95% confidence level intervals in the Ω_m-σ_8 plane derived from the shear correlation functions measured by the CFHTLenS survey. The solid blue line indicates the constraints obtained for the same dataset by Kilbinger et al. (2013), which follows the degeneracy of constant $\sigma_8^{-1}\Omega_{\rm m}^{0.6}$.

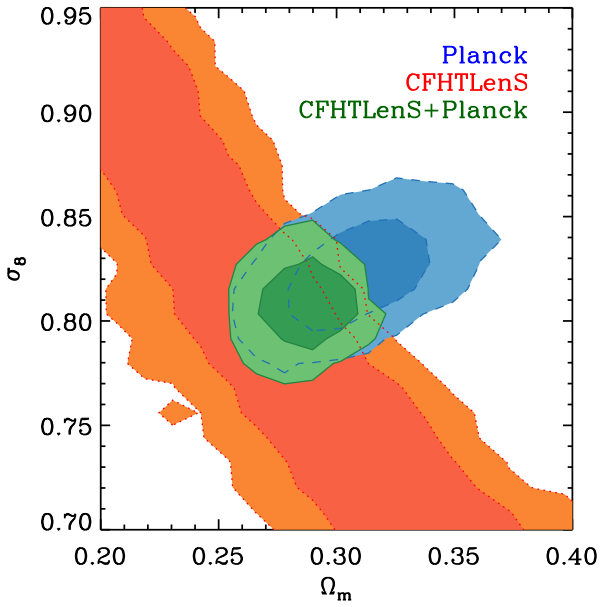

Figure 7. Marginalised constraints in the Ω_m-σ_8 plane. The dashed blue contours corresponds to the measurements from the Planck data, whereas the red contours shows the constraints from the CFHTLenS shear correlation functions. The green contours show the results when these two measurements are combined.

an improved version of the halofit code, which relies on the approximated fitting formula of Eisenstein & Hu (1998).

We can see that our constraints are very similar those of Kilbinger et al. (2013). In particular, the statistical uncertainty is almost identical between the two methods. The disagreement in the best fit combination is only a small fraction of the statistical uncertainty in the constraints. This validates our approach and confirms that our theoretical model is at least, at the same level of accuracy as the state-of-the-art. We emphasise though, that our formalism present many advantages over previous ones which will be likely relevant for future data analyses, as it has been discussed thorough our paper.

In Fig. 7, we combine our constraints with those obtained from CMB measurements. Specifically, we use the data described in §3.2 via publicly available chains[7], which is displayed by the blue contours.

There is a mild tension between the two datasets considered. However, this is not statistically significant. We thus combine the constraints by multiplying the respective likelihoods. The addition of Planck data breaks the degeneracy present in the CFHTLenS constraints, resulting in constraints much tighter than those from each of the methods individually. The marginalised best fit parameters we obtain are $\sigma_8 = 0.811 \pm 0.009$ and $\Omega_m = 0.290 \pm 0.011$, which is within the 1σ regions of each dataset.

Fig. 8 compares measured CFHTLenS shear correlation functions to those predicted by our method for these best fit parameters. We can see that the model is indeed a very good description of the data at all scales and for both ξ_+ and ξ_-, in particular if one keeps in mind the large covariance among the points and that this is not necessarily the best fit to the CFHTLenS data alone. We also recall that in §5.3, we carried out a direct N-body simulation with this specific set of parameters and found that our theoretical model was accurate at the $< 3-4\%$ level for this target cosmological model.

[7] `http://pla.esac.esa.int/pla/aio/product-action?COSMOLOGY.FILE_ID=COM_CosmoParams_base_planck_lowl_lowLike_highL_R1.10.tar.gz`

7 CONCLUSIONS

We have developed and explored a new formalism for an accurate and flexible cosmological exploitation of cosmic shear correlation functions. The core of the method is an improved version of the cosmology-scaling algorithm originally proposed by Angulo & White (2010).

We have explicitly demonstrated the accuracy of our approach by comparing its predictions with those derived from N-body simulations carried in extreme cosmological scenarios. We showed that shear correlation function can be predicted always with a $< 10\%$ accuracy, which is much smaller than the uncertainties in the data, and comparable with the theoretical uncertainties in N-body simulations and in the procedure to combine mass correlation functions into shear correlations.

The method can quickly provide, in about 4 seconds, predictions for shear correlation functions. We exploited this by coupling the algorithm with an MCMC sampler to obtain cosmological constraints on σ_8 and Ω_m from CFHTLenS data. The resulting constraints follow a degeneracy of constant $\sigma_8^{-1}\Omega_{\rm m}^{0.6} = 0.801 \pm 0.028$, which can be broken with the addition of CMB data. In this case, we obtain marginalised constraints $\sigma_8 = 0.811 \pm 0.009$ and $\Omega_m = 0.290 \pm 0.011$

Our results are very similar to published results, which rely in simpler (and likely less accurate) input nonlinear correlation functions. The current agreement is due to the still rel-

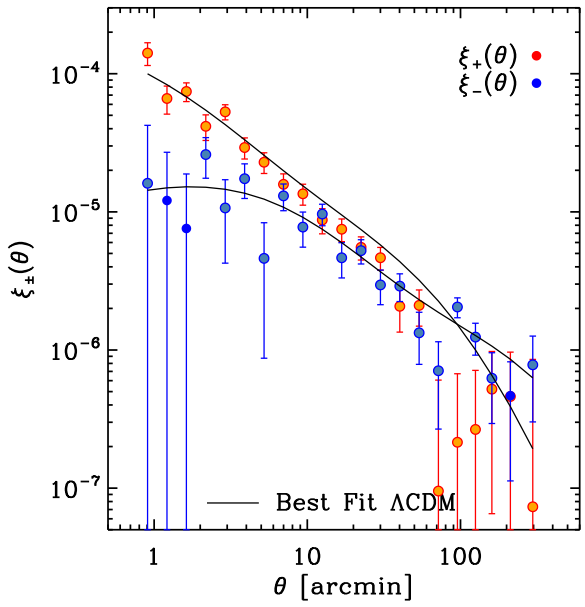

Figure 8. The cosmic shear correlation functions, $\xi_+(\theta)$ (red circles) and $\xi_-(\theta)$ (blue circles), as measured by the CFHTLenS survey. The error bars are given by the square root of the inverse of the respective covariance matrix. The solid lines show the best-fitting flat ΛCDM model to the shear correlation functions and to the CMB temperature anisotropies measured by the Planck satellite and the polarization measured by the WMAP satellite.

atively large statistical uncertainties associated with the data. This situation, however, will change in the foreseeable future with the arrival of several wide and deep weak lensing surveys, which will demand greater accuracy and sophistication in the cosmological analysis.

Here we have shown the basic feasibility of our framework. We foresee several developments building upon the unique features our method provides. In particular:

(1) The high accuracy in the predictions will further increase naturally as larger and higher-resolution N-body simulations arrive. Furthermore, simulations with different cosmological parameters can be combined to cover a large range in parameter space, for which the scaling yields two-point and higher-order correlation functions with a tight upper limit on their uncertainties.
(2) The continuous progress in computer hardware and algorithms should soon allow an incorporation of the large-scale structure correction into the MCMC chains. Similarly, eventually it should be possible to directly handle the full N-body outputs allowing, for instance, an on-the-fly light-cone construction.
(3) A full three-dimensionality in the predictions will be possible, which will allow to dynamically incorporate selection functions, masks appropriate of a given survey, and an accurate account for effects such as source-lens clustering.
(4) The dark matter halo and subhalo population will be resolved at each point of the cosmological parameter space. This could, in principle, enable a flexible and realistic account of baryonic effects (such as mass redistribution inside halos due to gas cooling and outflows), e.g. via a combination with galaxy formation models.

It is for all these characteristics that we anticipate that our method could be extremely useful to exploit the upcoming lensing data. A full realisation of its potential could change the way in which cosmological data is analysed, advancing considerably the state-of-the-art in terms of scope, sophistication and realism.

ACKNOWLEDGEMENTS

We thank Martin Kilbinger and Simon White for helpful comments.

We thank the CFHT staff and the members of the CFHTLenS collaboration for providing the CFHTLenS shear correlation data products to the astronomical community.

The CFHTLenS data used in this publication is based on observations obtained with MegaPrime/MegaCam, a joint project of CFHT and CEA/IRFU, at the Canada-France-Hawaii Telescope (CFHT) which is operated by the National Research Council (NRC) of Canada, the Institut National des Science de l'Univers of the Centre National de la Recherche Scientifique (CNRS) of France, and the University of Hawaii. This work is based in part on data products produced at Terapix available at the Canadian Astronomy Data Centre as part of the Canada-France-Hawaii Telescope Legacy Survey, a collaborative project of NRC and CNRS.

Author contributions: R.A. and S.H. planned the project, wrote the paper and interpreted the results. R.A. carried out the test simulations and the MS-I into the future, devised an improved cosmology-scaling algorithm, computed the 3D and shear correlation functions, and performed the cosmological analysis. S.H. derived the expressions for shear correlations from scaled mass correlation functions, carried out the ray-tracing simulations, computed projected mass and shear correlation functions, and performed systematics tests on these.

REFERENCES

Agarwal S., Abdalla F. B., Feldman H. A., Lahav O., Thomas S. A., 2014, MNRAS, 439, 2102
Angulo R. E., Springel V., White S. D. M., Jenkins A., Baugh C. M., Frenk C. S., 2012, MNRAS, 426, 2046
Angulo R. E., White S. D. M., 2010, MNRAS, 405, 143
Angulo R. E., White S. D. M., Springel V., Henriques B., 2013, ArXiv e-prints
Bacon D. J., Refregier A. R., Ellis R. S., 2000, MNRAS, 318, 625
Bartelmann M., 2010, Classical and Quantum Gravity, 27, 233001
Benjamin J. et al., 2013, MNRAS, 431, 1547
Boylan-Kolchin M., Bullock J. S., Kaplinghat M., 2011, MNRAS, 415, L40
Das S. et al., 2014, JCAP, 4, 14
Eisenstein D. J., Hu W., 1998, ApJ, 496, 605
Erben T. et al., 2013, MNRAS, 433, 2545
Fu L. et al., 2014, ArXiv e-prints
Fu L. et al., 2008, A&A, 479, 9
Habib S., Heitmann K., Higdon D., Nakhleh C., Williams B., 2007, Phys. Rev. D, 76, 083503
Heitmann K., Lawrence E., Kwan J., Habib S., Higdon D., 2014, ApJ, 780, 111
Heitmann K., White M., Wagner C., Habib S., Higdon D., 2010, ApJ, 715, 104

Heymans C. et al., 2012, MNRAS, 427, 146
Hilbert S., Hartlap J., Schneider P., 2011, A&A, 536, A85
Hilbert S., Hartlap J., White S. D. M., Schneider P., 2009, A&A, 499, 31
Hildebrandt H. et al., 2012, MNRAS, 421, 2355
Hinshaw G. et al., 2013, ApJS, 208, 19
Hoekstra H. et al., 2006, ApJ, 647, 116
Hoekstra H., Yee H. K. C., Gladders M. D., 2002, ApJ, 577, 595
Huff E. M., Eifler T., Hirata C. M., Mandelbaum R., Schlegel D., Seljak U., 2014, MNRAS, 440, 1322
Jee M. J., Tyson J. A., Schneider M. D., Wittman D., Schmidt S., Hilbert S., 2013, ApJ, 765, 74
Kaiser N., 1992, ApJ, 388, 272
Kilbinger M., Benabed K., Coupon J., McCracken H. J., Fu L., 2012, NumerIcal Cosmology And lEnsing cAlculations (NICAEA) version 2.4. http://www2.iap.fr/users/kilbinge/nicaea/
Kilbinger M. et al., 2013, MNRAS, 430, 2200
Kitching T. D. et al., 2014, ArXiv e-prints
Kuhlen M., Vogelsberger M., Angulo R., 2012, Physics of the Dark Universe, 1, 50
Lewis A., Challinor A., Lasenby A., 2000, ApJ, 538, 473
Ludlow A. D., Navarro J. F., Angulo R. E., Boylan-Kolchin M., Springel V., Frenk C., White S. D. M., 2013a, ArXiv e-prints
Ludlow A. D. et al., 2013b, MNRAS, 432, 1103
Mead A. J., Peacock J. A., 2014, MNRAS, 440, 1233
Miller L. et al., 2013, MNRAS, 429, 2858
Peacock J. A., Dodds S. J., 1996, MNRAS, 280, L19
Planck Collaboration et al., 2013, ArXiv:1303.5076
Refregier A., Rhodes J., Groth E. J., 2002, ApJ, 572, L131
Ruiz A. N., Padilla N. D., Domínguez M. J., Cora S. A., 2011, MNRAS, 418, 2422
Sato M., Hamana T., Takahashi R., Takada M., Yoshida N., Matsubara T., Sugiyama N., 2009, ApJ, 701, 945
Schneider M. D., Holm Ó., Knox L., 2011, ApJ, 728, 137
Schneider P., Kochanek C., Wambsganss J., 2006, Gravitational Lensing: Strong, Weak and Micro, Saas-Fee Advanced Course 33. Springer, Berlin
Schneider P., van Waerbeke L., Mellier Y., 2002, A&A, 389, 729
Schrabback T. et al., 2010, A&A, 516, A63
Seljak U., 2000, MNRAS, 318, 203
Semboloni E., Schrabback T., van Waerbeke L., Vafaei S., Hartlap J., Hilbert S., 2011, MNRAS, 410, 143
Smith R. E. et al., 2003, MNRAS, 341, 1311
Springel V. et al., 2005, Nature, 435, 629
Story K. T. et al., 2013, ApJ, 779, 86
Takahashi R., Sato M., Nishimichi T., Taruya A., Oguri M., 2012, ApJ, 761, 152
Tyson J. A., Wenk R. A., Valdes F., 1990, ApJ, 349, L1
van Daalen M. P., Schaye J., Booth C. M., Dalla Vecchia C., 2011, MNRAS, 415, 3649
van Daalen M. P., Schaye J., McCarthy I. G., Booth C. M., Vecchia C. D., 2014, MNRAS, 440, 2997
White M., Vale C., 2004, Astroparticle Physics, 22, 19
Wilson G., Kaiser N., Luppino G. A., Cowie L. L., 2001, ApJ, 555, 572
Wittman D. M., Tyson J. A., Kirkman D., Dell'Antonio I., Bernstein G., 2000, Nature, 405, 143
Zentner A. R., Semboloni E., Dodelson S., Eifler T., Krause E., Hearin A. P., 2013, Phys. Rev. D, 87, 043509